Bull. Mater. Sci., Vol. 40, No. 1, February 2017, pp. 55–66. © Indian Academy of Sciences.
DOI 10.1007/s12034-017-1361-9

Modelling, structural, thermal, optical and vibrational studies of a new organic–inorganic hybrid material $(C_5H_{16}N_2)Cd_{1.5}Cl_5$

MELEK HAJJI[1], CHIRAZ KOURAICHI[2] and TAHA GUERFEL[1,3,*]

[1]Laboratoire d'Electrochimie, Matériaux et Environnement, Université de Kairouan, 3100 Kairouan, Tunisia
[2]Institut Supérieur d'Informatique et de Multimédia de Gabès, Campus Universitaire-BP 122, 6033 Cité El Amel 4, Gabès, Tunisia
[3]Institut Préparatoire aux Etudes d'Ingénieurs de Kairouan, 3100 Kairouan, Tunisia

MS received 18 October 2015; accepted 24 June 2016

Abstract. **Chemical preparation, theoretical calculations, X-ray single-crystal diffraction, thermal analysis, electrochemical measurements, IR, Raman and UV spectroscopic investigations of a novel organic–inorganic hybrid material $(C_5H_{16}N_2)Cd_{1.5}Cl_5$ are described. The structure provides a new interesting example of infinite inorganic chains of $[Cd_{1.5}Cl_5]_n^{2n-}$ following the *a* crystallographic direction. The $[Cd_{1.5}Cl_5]^{2-}$ anions are interconnected by N–H$\cdots$Cl hydrogen bonds. The Hirshfeld surface and associated fingerprint plots of the compound are presented to explore the nature of intermolecular interactions and their relative contributions in building the solid-state architecture. IR and Raman spectra are reported and discussed on the basis of group theoretical analysis and quantum chemical density functional theory (DFT) calculation. The molecular HOMO–LUMO compositions and their respective energy gaps are also drawn to explain the activity of our compound. Thermal analysis reveals the anhydrous character of the compound.**

Keywords. **Crystal structure; vibrational spectroscopy; DFT calculations; thermal analysis (TG–DTA).**

1. Introduction

Recently, much attention has been devoted to the large family of organic–inorganic metal halides due to their particular structural features and physical properties. This important class of low-dimensional materials displays distinctive optical properties such as strong and sharp photoluminescence, electroluminescence and highly efficient nonlinear optical effects [1–3]. Some interest has been directed towards halocadmates (II) compounds in combination with organic cation, due to the potential semiconducting behaviour, as well as the wealthy structural diversity displayed by these systems. As already pointed out in several published works, the structural chemistry of cadmium chloride in the solid states has numerous structures mainly with an anionic sublattice built up of the $CdCl_6$, which can be connected in one of three ways: face, edge or corner sharing, forming naturally isolated molecules (0D), infinite chains (1D) and two (2D) or three (3D)-dimensional networks [4–7]. The cavities between the inorganic moieties are filled with organic cations that connect to the anionic framework through hydrogen bonds and/or electrostatic interactions [8,9]. On the other hand, there is still growing interest in the study of crystals containing alkylammonim. The specific geometry of these cations can generate supramolecular networks in one, two or three dimensions [10,11]. In this work, we synthesized a novel alkylammonium-chlorocadmate compound $(C_5H_{16}N_2)Cd_{1.5}Cl_5$. The polymeric complex was characterized by X-ray diffraction, TG–DTA measurement, FT-IR absorption and FT-Raman scattering. Using the cyclic voltammetry, some electrochemical measurements are reported. The 3D Hirshfeld surfaces and the associated 2D fingerprint plots were investigated for intermolecular hydrogen bonding interactions [12,13].

2. Experimental

2.1 *Chemical preparation*

Crystals of catena-bis(3-dimethylammoniopropylammonium) decakis(μ_2-chloro)-tri-cadmium(II) were prepared by slow evaporation, at room temperature, of 400 ml of an aqueous solution of HCl (0.04 mol, 3.28 ml, purity 37%, Aldrich) mixed with 5.5 g of $CdCl_2$ (3×10^{-2} mol, purity 98%, Aldrich) and neutralized by 2×10^{-2} mol of 3-dimethylaminopropylamine (2.22 ml, purity 99%, Aldrich). During this operation, the solution was vigorously stirred. Scheme 1 gives the main steps of the preparation of $(C_5H_{16}N_2)Cd_{1.5}Cl_5$. When most of the solution was evaporated, elongated transparent colourless prisms (average size, 0.25 mm $\times$ 0.33 mm $\times$ 0.41 mm) were obtained.

*Author for correspondence (taha_guerfel@yahoo.fr)

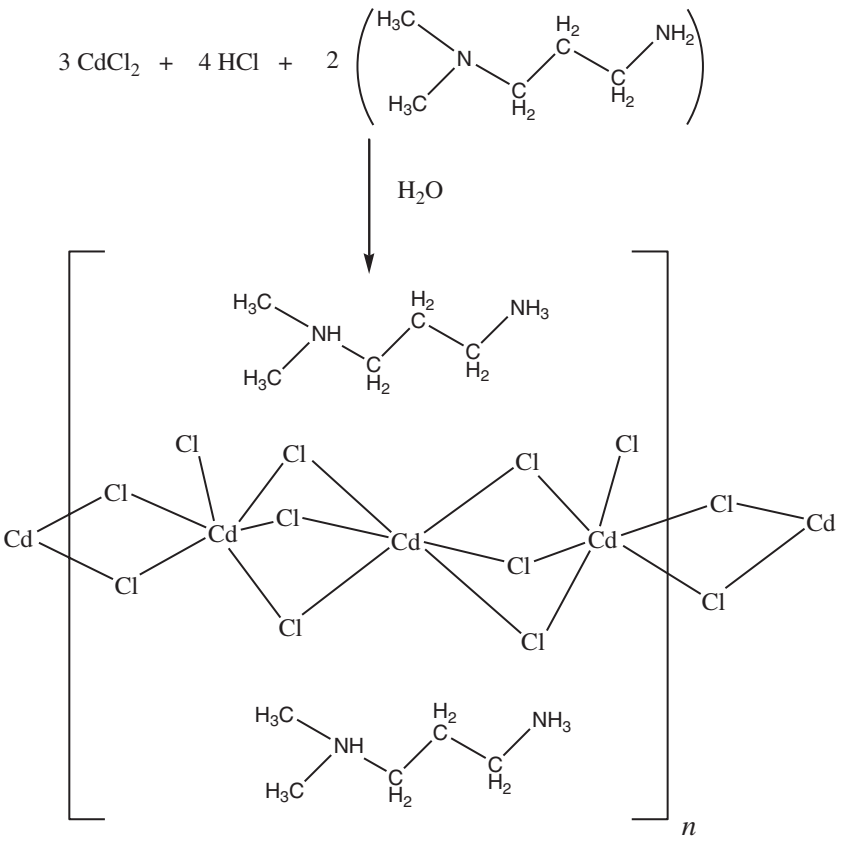

Scheme 1. Synthesis of $(C_5H_{16}N_2)Cd_{1.5}Cl_5$.

2.2 *Single-crystal X-ray diffraction*

Single-crystal X-ray diffraction measurements were carried out at 293 K on a Bruker Enraf-Nonius diffractometer using graphite monochromatized Mo Kα radiation in the ω–2θ scan mode. Final unit cell dimensions were obtained and refined using a set of 25 high-angle reflections. Integration and scaling resulted in the data set, corrected for Lorentz and polarization effects using XCAD4 [14]. The structure of catena-bis(3-dimethylammoniopropylammonium)-decakis(μ_2-chloro)-tri-cadmium(II) was developed in the centrosymmetric space group $P2_1/c$. The trial structure was obtained by direct methods using SHELXS-97 [15], which revealed the position of the cadmium, chlorine and most atoms of the organic molecule. The remainder of the structure was found in the subsequent difference Fourier syntheses. There are one $[Cd_{1.5}Cl_5]^{2-}$ anion and one organic $(C_5H_{16}N_2)^{2+}$ cation. The final structural refinement was made with F^2 data using the program SHELXL-97 [15]. All the hydrogen positions of the diprotonated cation were placed geometrically and held in the riding mode. Anisotropic displacement parameters for all the other atoms were allowed to vary. The anisotropies were found to be moderate. Crystal data and the results of the final structure refinement are summarized in table 1. Selected bond distances and angles are listed in tables 2 and 3.

2.3 *Spectroscopic measurements*

Infrared (IR) spectrum was recorded at room temperature on a Biored FTS 6000 FTIR spectrophotometer in the 400–4000 cm^{-1} region. Thin transparent pellets were made by compacting an intimate mixture obtained by shaking 2 mg of the sample in 100 mg of KBr. Raman spectrum was recorded on a Jobin Yvon Horiba HR800 LabRAM spectrometer in the range of 200–2000 cm^{-1}. UV–vis spectrum was measured using a high-resolution Beckman DU640 spectrophotometer in the 200–800 nm range using aqueous solution.

2.4 *Thermal behaviour*

A Setaram TG–DTA 92 thermoanalyser was used to perform a thermal treatment on $(C_5H_{16}N_2)$ $Cd_{1.5}Cl_5$. TG–DTA thermograms were obtained with a 20.2 mg sample in an open platinum crucible heated in the air at 5°C min^{-1} from room temperature to 450°C. An empty crucible was used as the reference.

2.5 *Cyclic voltammetry analyses*

Electrochemical measurements were performed in a conventional electrochemical cell containing a three-electrode

Table 1. Crystal data and structure refinement of $(C_5H_{16}N_2)Cd_{1.5}Cl_5$.

Compound	$(C_5H_{16}N_2)Cd_{1.5}Cl_5$
Crystal system	Monoclinic
Space group	$P2_1/c$
Molar mass	450.05 g mol^{-1}
Temperature	293 (2) K
Radiation used	0.71073 Å
Unit cell parameters	$a = 10.1393(4)$ Å
	$b = 13.9493(5)$ Å; $\beta = 112.627(8)°$
	$c = 10.6629(4)$ Å
V/Z	1392.04(9) Å^3/ 4
$\rho_{calculated}$	2.147 g cm^{-3}
Absorption coefficient	3.237 mm^{-1}
$F(000)$	868
Crystal dimensions	$0.25 \times 0.33 \times 0.41$ mm^3
Colour/shape	Colourless/prismatic
Diffractometer	CAD4
Wavelength	Mo K_α ($\lambda = 0.71073$ Å)
Scan mode	$\omega/2\theta$
Theta range (θ)	2.18–24.97°
h, k, l range	$-12 \leq h \leq 11$; $-2 \leq k \leq 16$; $0 \leq l \leq 12$
Program data reduction	XCAD4 [14]
Number of reflections measured	3045
Number of reflections observed	2444
Absorption correction	SHELXA [15]
Maximum/minimum transmission	0.5637/0.3575
Structure resolution	Direct method: SHELXS-97 [15]
Structure refinement	Based on F^2: SHELXL-97 [15]
Restraints/independent parameters	0/125
Extinction coefficient = 0.0307(16)	$S = 1.126$
Final R indices [$I > 2\sigma(I)$]	0.0445
wR_2^b	0.1187
$\Delta\rho_{min}/\Delta\rho_{max}$ (e Å^{-3})	−1.363/1.331

$R_1^a = \frac{\Sigma||F_o|-|F_c||}{\Sigma|F_o|}$, $wR_2^b = \left[\frac{\Sigma w(F_o^2-F_c^2)^2}{\Sigma w(F_o^2)^2}\right]^{1/2}$ and $w = \frac{1}{\sigma^2(F_o^2)+(0.0251P)^2+3.91P}$, where $P = \frac{F_o^2+2F_c^2}{3}$.

system, ensuring stable positioning of the electrodes and an agitation of the solution. The glassy carbon electrode was the working electrode, a platinum electrode was an auxiliary electrode and a saturated calomel electrode served as a reference electrode.

3. Computational details

The molecular structure of our compound was fully optimized without any constraint using the density functional theory (DFT) approach and effective core potentials (ECPs) in order to represent the metal (LANL2DZ basis and ECP built-in). The B3LYP method with 6-31+G(d,p) basis set was used for all atoms except for cadmium [16–18]. Harmonic vibrational frequencies and their corresponding vibrational intensities were also computed using the same functional and basis set. The molecular geometry was not limited

Table 2. Experimental (X-ray) and calculated geometric parameters of $(C_5H_{16}N_2)$ organic cation.

Geometric parameters	Experimental values	Calculated values
	Organic cations	
Bond lengths (Å)		
N(1)–C(1)	1.492(7)	1.523
N(2)–C(3)	1.499(7)	1.536
N(2)–C(4)	1.505(7)	1.524
N(2)–C(5)	1.488(7)	1.522
C(1)–C(2)	1.517(7)	1.540
C(2)–C(3)	1.504(7)	1.542
Bond angles (°)		
C(3)–N(2)–C(4)	109.9(5)	108.1
C(3)–N(2)–C(5)	112.8(4)	112.0
C(4)–N(2)–C(5)	111.3(5)	109.6
N(2)–C(3)–C(2)	111.6(4)	114.3
C(1)–C(2)–C(3)	111.9(4)	111.2
N(1)–C(1)–C(2)	108.0(4)	112.9

Table 3. Bond lengths (Å) and angles (°) in $CdCl_6$ octahedra.[a]

			$[Cd(1)Cl_6]^{1-}$			
Cd1	Cl1	Cl1(i)	Cl2	Cl2(i)	Cl3	Cl3(i)
Cl1	**2.647(1)**	**5.295(2)**	3.546(3)	3.839(1)	3.633(1)	3.931(2)
Cl1(i)	180.00	**2.647(1)**	3.839(1)	3.546(3)	3.931(2)	3.633(1)
Cl2	85.44(4)	94.56(4)	**2.578(1)**	**5.157(5)**	3.435(2)	4.016(2)
Cl2(i)	94.56(4)	85.44(4)	**180.00**	**2.578(1)**	4.016(2)	3.435(2)
Cl3	85.48(3)	94.52(3)	81.07(4)	98.93(4)	**2.704(1)**	**5.409(2)**
Cl3(i)	94.52(3)	85.48(3)	98.93(4)	81.07(4)	**180.00**	**2.704(1)**
	$DI[Cd-Cl]=0.016$		$DI[Cl-Cl]=0.052$		$DI[Cl-Cd-Cl]=0.062$	
			$[Cd(2)Cl_6]^{1.5-}$			
Cd2	Cl1	Cl2	Cl3	Cl4	Cl5	Cl5(ii)
Cl1	**2.708(1)**	3.546(3)	3.633(1)	3.804(1)	**5.317(3)**	3.825(2)
Cl2	81.21(4)	**2.738(1)**	3.435(2)	**5.278(2)**	3.887(1)	3.832(2)
Cl3	84.64(4)	78.56(4)	**2.687(1)**	3.791(2)	3.916(2)	**5.245(1)**
Cl4	92.35(4)	**169.33(4)**	92.44(4)	**2.563(1)**	3.770(3)	3.835(2)
Cl5	**174.20(4)**	93.07(4)	95.23(4)	93.45(4)	**2.615(1)**	3.557(1)
Cl5(ii)	92.71(4)	92.26(4)	**170.72(4)**	96.56(4)	86.50(4)	**2.575(1)**
	$DI[Cd-Cl]=0.024$		$DI[Cl-Cl]=0.035 DI$		$[Cl-Cd-Cl]=0.053$	

• Bold values indicate distances and angles between diametrically opposed atoms (relative to the cadmium atom).
• Bold underlined values indicate distances between Cd and Cl atoms.
• Italic values indicate distortion indices.
[a]Symmetry operators:
(i) $-x, -y+1, -z+1$
(ii) $-x-1, -y+1, -z+1$

and all the calculations (vibrational wavenumbers, optimized geometric parameters and other molecular properties) were performed using the GaussView molecular visualization program and Gaussian 09W program package [19,20]. Furthermore, the calculated vibrational frequencies were clarified by means of the potential energy distribution (PED) analysis of all the fundamental vibration modes using the VEDA 4 program [21]. Scaling factors used in this study were taken from literature [22]. In order to take into account the effect of intermolecular interactions on geometrical parameters and vibrational spectroscopy, we have considered an appropriate cluster model built up from one $[Cd_3Cl_{10}]^{4-}$ anion and two organic $(C_5H_{16}N_2)^{2+}$ cations linked by N–H$\cdots$Cl hydrogen bonds. Molecular Hirshfeld surfaces and the associated fingerprint information were calculated using the CrystalExplorer 3.0 software [23]. All bond lengths to hydrogen were automatically modified to typical standard neutron values (C–H = 1.083 Å and N–H = 1.009 Å), while the CIF file of crystal was read into the CrystalExplorer software program for calculations [24].

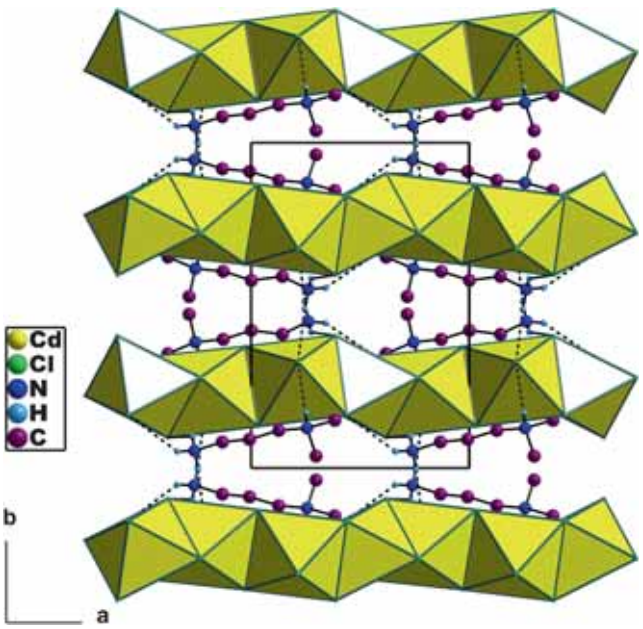

Figure 1. Projection along the *c*-axis of the atomic arrangement (for clarity, the H atoms of carbon are omitted; H-bonds are represented by dashed lines).

4. Results and discussion

4.1 *Structure description*

The atomic arrangement of catena-bis(3-dimethylammoniopropylammonium) decakis(μ_2-chloro)-tri-cadmium(II) is described by a three-dimensional stacking of hydrogen bonds binding the different entities of the structure. The projection of the atomic arrangement along the *c*-axis shows $[CdCl_6]^{-}$ anions sharing two faces with two neighbour $[CdCl_6]^{1.5-}$ anions (figure 1). Each $[CdCl_6]^{1.5-}$ octahedron shares one edge and one face with the two neighbouring anions to form chains of formulas: $[Cd_{1.5}Cl_5]_n^{2n-}$ parallel to the *a*-axis. Interconnection between different chains is insured by N–H$\cdots$Cl hydrogen bonds (figure 2). Each $[Cd_{1.5}Cl_5]^{2-}$ anion

is surrounded by three organic molecules delivering four hydrogen bonds. Interatomic distances and angles describing the two $CdCl_6$ octahedra are reported in table 3. The Cd–Cl and Cl–Cl (with Cl in *cis*-positions) distances vary, respectively, from 2.563(1) to 2.738(1) Å and from 3.435(2) to 4.016(2) Å. The slight differences between Cd–Cl distances are due to the different environments of chlorine atoms. The detailed geometry of $[Cd_{1.5}Cl_5]^{2-}$ anions indicates that among the Cd–Cl distances, two different types are distinguished: the longest corresponds to the bridging chlorine atoms and the shortest relates to the external chlorine atoms. The Cl–Cd–Cl angles (with Cl in *cis*-positions) vary from 78.56(4) to 98.93(4)°. The calculation of angles and distances distortion indices in $CdCl_6$ octahedra, according to the Baur method [25], shows a more pronounced distortion of Cl–Cd–Cl angles when compared with Cd–Cl and Cl–Cl distances. The $[Cd(1)Cl_6]^{1.5-}$ octahedron, which shares one edge and one face with the two neighbouring anions, shows the most pronounced distortion in the Cd–Cl distances (table 3). The $[Cd(2)Cl_6]^{1-}$ anion, which shares two faces, presents the most pronounced distortion in the Cl–Cl distances. The protonation of organic molecule, according to the experimental protocol, led to the 3-dimethylammoniopropylammonium cation with the protonation of the two nitrogen atoms. From experimental (X-ray) and calculated geometric parameters of the organic molecule shown in table 2, it is illustrated that some of the calculated bond lengths and bond angles using the 'B3LYP/LANL2DZ approach' are found to be slightly different from the experimental values. These discrepancies may be due to the presence of intermolecular hydrogen bonding. It can also be explained by the fact that the calculations relate to the isolated molecule where the intermolecular Coulombic interactions with the neighbouring molecules are absent, whereas the experimental result corresponds to interacting molecules in the crystal lattice. The C–C distances vary between 1.504(7) and 1.517(7) Å with an average distance ⟨C–C⟩ of 1.511 Å. The C–N distances vary between 1.488(7) and 1.505(7) Å with an average value ⟨C–N⟩ of 1.496 Å. The angles vary between: 108.0(4) and 112.8(4)° with an average value of 110.9°. The interatomic distances and angles describing this cation are similar to intramolecular bond distances and angles usually reported for such species [10]. Through its protons, each nitrogen atom of the organic cation shares hydrogen bonds of N–H···Cl type with chlorine atoms, thus forming the crystalline structure. Figure 2 shows that each organic molecule is simultaneously linked to two $[Cd_{1.5}Cl_5]_n^{2n-}$ chains. The geometrical parameters of these bonds are reported in table 4. According to the criterion relating to the N···Cl distances, all the N–H···Cl hydrogen bonds are considered weak. Indeed, N···Cl distances vary between 3.221(4) and 3.334(5) Å [26]. The crystalline structure does not contain the same number of donors and acceptors involved in the hydrogen bonding system: four N(H) as donors, three chlorine as acceptors. Cl1 and Cl3 atoms are simply acceptors, Cl4 atom is a double acceptor. Cohesion and stability of crystalline building are maintained by the 3D network of hydrogen bonds.

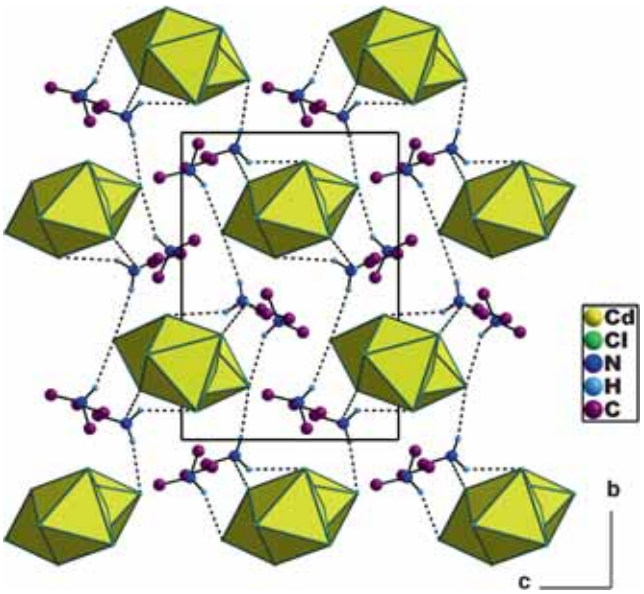

Figure 2. Projection along the *a*-axis of the atomic arrangement (for clarity, the H atoms of carbon are omitted; H-bonds are represented by dashed lines).

4.2 *Hirshfeld surfaces analysis*

The molecular Hirshfeld surfaces of $[Cd_3Cl_{10}]^{4-}$ were generated using a standard (high) surface resolution. The 3D d_{norm} surfaces were mapped over a fixed colour scale of

Table 4. Bond lengths (Å) and angles (°) in the hydrogen-bonding scheme.[a]

	N–H	H···Cl	N···Cl	N–H···Cl
N(1)–H(1N1)···Cl3$^{(i)}$	0.890	2.592	3.334(5)	141.35
N(1)–H(2N1)···Cl1	0.890	2.601	3.268(5)	132.45
N(1)–H(3N1)···Cl4$^{(ii)}$	0.890	2.404	3.291(4)	174.64
N(2)–H(1N2)···Cl4$^{(iii)}$	0.910	2.372	3.221(4)	155.19

[a]Symmetry operators:
(i) $-x, -y+1, -z+1$
(ii) $-x, y-1/2, -z+3/2$
(iii) $x+1, y, z$

−0.453 (red) to 1.242 (blue) (figure 3a) and the shape index surfaces were mapped in the colour range of −0.998 to 0.998 (figure 3b). The hydrogen bonds interactions are also evident in shape index by a red concave region around the acceptor atom. The 2D fingerprint plots can be decomposed to highlight particular atom pair close contacts [27]. This decomposition enables separation of contributions from different interaction types that overlap in the full fingerprint (figure 4a). The Cl···H intermolecular interactions appear as a spike pointing towards the lower left of the plot (figure 4b). Complementary regions are visible in the fingerprint plots where one molecule acts as a donor ($de > di$) and the other as an acceptor ($de < di$). The shortest contact, i.e., the minimum value of ($de + di$) is around 2.3 Å; this points out the importance of these interactions. The proportion of Cl···H interactions comprises 38% of the total Hirshfeld surfaces. The Cl···C intermolecular interactions appear as a small spike, which have the most significant contribution to the total Hirshfeld surfaces, comprising 44.4% (figure 4c). At the top left and middle right of the fingerprint plot, there are characteristic 'wings', which are identified as a result of Cl···Cd/Cd···Cl interactions (figure 4d). The decomposition of the fingerprint plot shows that Cl···Cd contacts comprise 7.9% of the total Hirshfeld surface area. The proportion of Cl···Cl interactions comprises 9.4% of the total (figure 4e). Thus, the nature of the interplay of the title compound is more easily understood using the Hirshfeld surface, with the results further highlighting the power of the technique in mapping out the interactions within the crystal, and this methodology has very important promise in crystal engineering.

4.3 *Frontier molecular orbital analysis*

The frontier molecular orbitals, termed the highest occupied molecular orbital (HOMO) and the lowest unoccupied molecular orbital (LUMO), play a significant role in the electric and optical properties, as well as in UV–vis spectra and chemical reactions. These orbitals determine the way the molecule interacts with other species. The LUMO as an electron acceptor represents the aptitude to obtain an electron, but HOMO represents the ability to donate the electron. The energy gap between HOMO and LUMO is a critical parameter in determining the electrical transport properties of molecules [28]. Recently, the energy gap has been used to demonstrate the bioactivity from intermolecular charge transfer [29,30]. A molecule with a small-scale frontier orbital gap is more polarizable and is generally associated with high chemical reactivity and low kinetic stability. It is also called as a soft molecule [31]. The contour surfaces of the frontier molecular orbitals are depicted in figure 5. The HOMO and LUMO are localized on the $[Cd_{1.5}Cl_5]^{4-}$ anion. The LUMO energy is 2.01 eV and the HOMO energy is −0.41 eV. The HOMO–LUMO gap (E_{LUMO}–E_{HOMO}) of $(C_5H_{16}N_2)Cd_{1.5}Cl_5$ is found to be 2.42 eV, obtained by the DFT method using B3LYP/LANL2DZ approach. The low value for frontier orbital gap has a substantial impact on the intramolecular charge transfer and the bioactivity of the molecule.

4.4 *UV–visible absorption spectroscopy*

The electronic spectrum shown in figure 6 reveals an absorption band centred at 383 nm (3.25 eV, 26109 cm^{-1}, $\varepsilon_{max} = 10845\ mol^{-1}\ cm^{-1}$); this band is due to the band gap absorption and it is assigned to the excitation of free electron–hole pairs within the $[CdCl_6]$ octahedron. This peak is mainly due to the absorption between Cl (3p) and Cd (5s) (band–band), which suggests that the material behaves as a semiconductor [32].

4.5 *Vibrational study*

In order to give more information about the crystal structure, we studied the vibrational properties of our compound using Raman scattering and IR absorption. Taking into account the effect of intermolecular interactions on geometrical parameters, we considered the $[Cd_3Cl_{10}]^{4-}$ anion and two organic cations linked via N–H···Cl hydrogen bond. All the parameters were allowed to relax and all the calculations converged to an optimized geometry, which corresponds to an energy minimum as affirmed by the lack of imaginary values in the calculated wavenumbers. The vibrational modes were supervised by the visual inspection of modes animated using the GaussView5.0 program and by comparison with experimental results reported in the literature for analogous compounds [19]. The computed wavenumbers

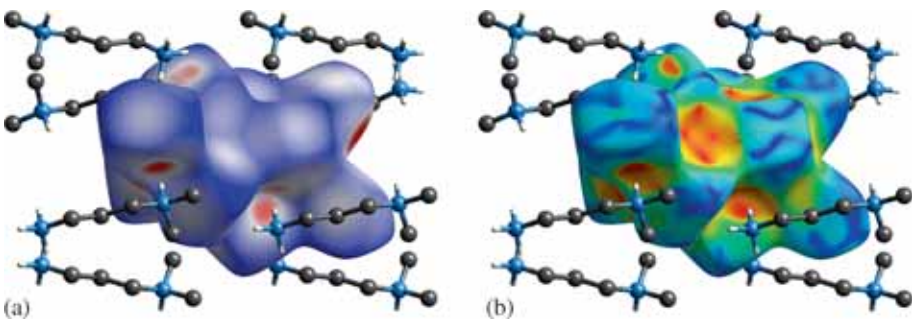

Figure 3. Hirshfeld surfaces mapped with (**a**) d_{norm} and (**b**) surface index.

corresponding to different modes along with detailed assignments are listed in table 5. For visual comparison, the observed and simulated Raman and IR spectra are presented, respectively, in figures 7 and 8.

The splitting of F_{1u} stretching mode of $CdCl_6$ into three components at 384, 370 and 361 cm^{-1} in the Raman spectrum depicted in figure 7 corroborates the symmetry lowering of $CdCl_6$ in the solid state towards the C_1 symmetry [33].

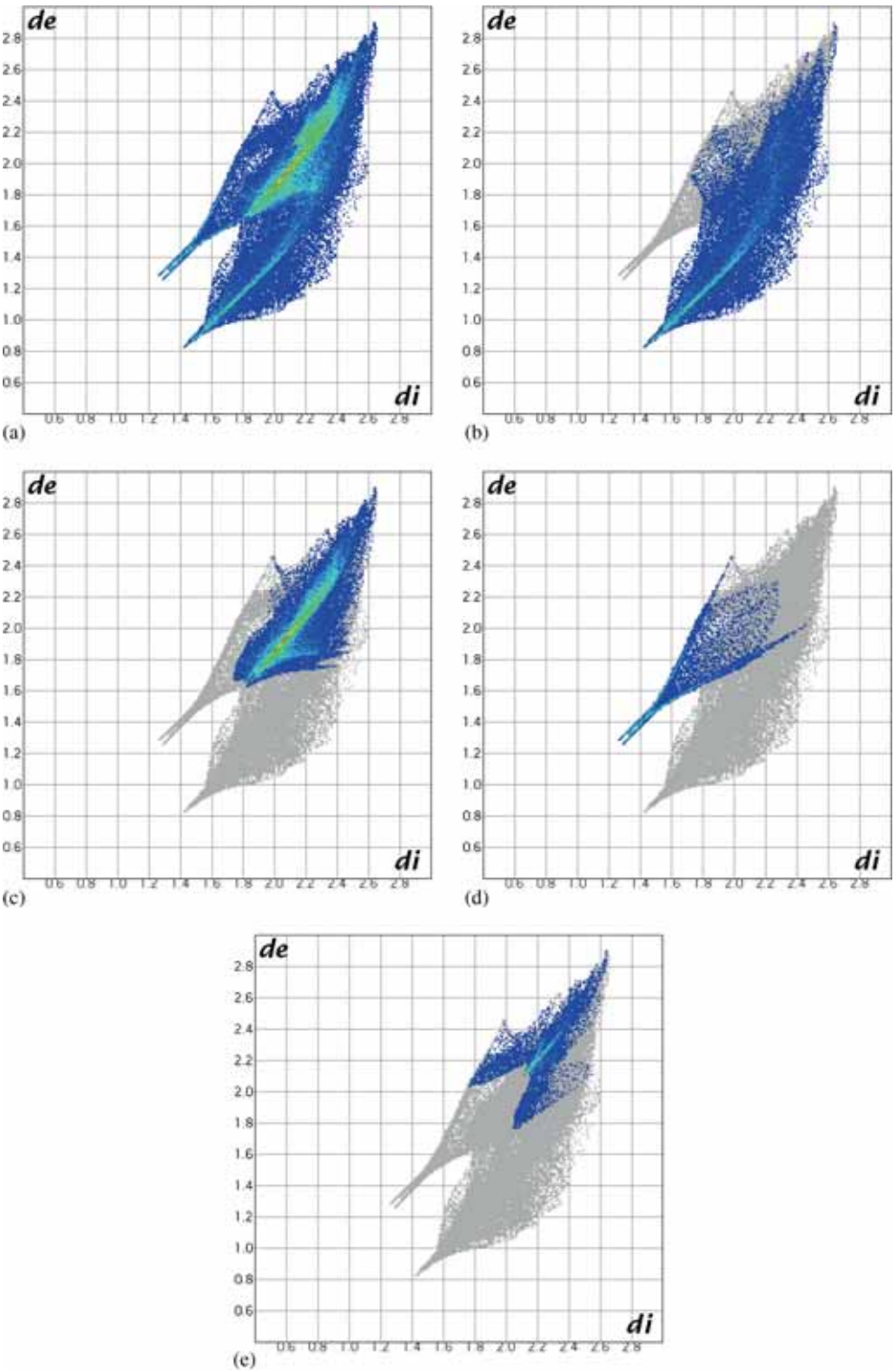

Figure 4. 2D fingerprint plots: (**a**) full and (**b**) resolved into Cl· · · H, (**c**) Cl· · · C, (**d**) Cl· · · Cd/Cd· · · Cl and (**e**) Cl· · · Cl contacts, showing the percentages of contacts contributed to the total Hirshfeld surface area of molecule.

The symmetric stretching modes $\nu_1(A_{1g})$ and $\nu_2(E_g)$ are found, respectively, as one peak at 351 cm^{-1} and two peaks at 272 and 231 cm^{-1}. Bending modes are observed at lower frequencies. The F_{2g} bending mode of $CdCl_6$ splits into three components at 185, 159 and 120 cm^{-1} in the Raman spectrum.

Numerous functional and skeletal groups such as CH_3, CH_2, NH_3, NH, N–C, C–C, CNC, NCC and CCC are present in 3-dimethylammoniopropylammonium cation. These groups are manifested in IR and Raman spectra in different ranges with different intensities. For the assignments of CH_3 and NH_3 groups, nine modes of vibration can be associated with each group, which are distributed as follows: one symmetric stretching (υ_s), two asymmetric stretching (υ_{as}), one symmetrical deformation (δ_s), two asymmetrical deformation (δ_{as}), one in-plane rocking (ρ_i), one out-of-plane rocking (ρ_o) and one twisting (τ) vibration modes. For the methyl and ammonium groups, the IR bands observed, respectively, at 3069, 3019 cm^{-1} and 3185 cm^{-1} are asymmetric stretching. The symmetric CH_3 and NH_3 stretching bands appeared, respectively, at 2944 and 3121 cm^{-1}. The asymmetric deformation modes for this groupment appeared in the range 1460–1520 cm^{-1}. The CH_3 deformation absorption occurs at 1411 cm^{-1}. This vibration is known as the umbrella mode that overlaps with CN ring stretching vibrations for the title compound. For the assignments of CH_2 group frequencies, basically six fundamentals can be associated with each CH_2 group, namely CH_2 symmetric stretch, CH_2 asymmetric stretch, CH_2 scissoring and CH_2 rocking, which includes in-plane vibrations and two out-of-plane vibrations, viz., CH_2 wagging and CH_2 twisting modes, which are expected to be depolarized [34]. The asymmetric CH_2 stretching vibrations are generally observed above 3000 cm^{-1}, while the symmetric stretch appears in the region 3000 and 2900 cm^{-1} [35,36]. In this study, the asymmetric stretching vibrations are observed at 3038 and 2944 cm^{-1} in FT-IR. Symmetric stretching vibration is observed at 2899 cm^{-1} in IR spectrum. The CH_2 scissoring mode has been assigned at 1224 cm^{-1} in Raman spectrum [37,38]. The band at 1177 cm^{-1} in IR spectrum is assigned to CH_2 in-plane rocking vibration [39]. The CH_2 wagging and CH_2 twisting vibrations are observed, respectively, at 272 and 159 cm^{-1} in Raman spectrum. The N–H stretching vibration is very sensitive to inter- and intramolecular hydrogen bonds and lies in the region 3300–3500 cm^{-1} in FT-IR spectrum. It gives rise to the vibrations as stretching vibration. Experimental and theoretical results show that 3100–3500 and 2756 cm^{-1} absorption bands are attributed to the ν(N–H) stretching vibration, which broadens owing to the formation of intermolecular N–H$\cdots$Cl hydrogen bonding in the structure. The band observed at 1520 cm^{-1} was assigned to experimental N–H rocking vibration for the title compound. The Raman bands observed at 1591, 1279 cm^{-1} and the corresponding IR bands at 1621, 1251 cm^{-1} can be assigned to C–N stretching mode. This mode is well reproduced by DFT calculations at 1640 and 1251 cm^{-1}. The band located at 1580 cm^{-1} in Raman spectrum and 1576 cm^{-1} in IR spectrum is assigned to C–N stretching mode coupled with C–C stretching mode. The C–C stretching vibrations of the title compound are found at 1208, 911 cm^{-1} in FTIR and 1253, 885 cm^{-1} in FT Raman. Their corresponding theoretically computed values are 1204 and 897 cm^{-1}, respectively. The C–C–N vibrational bands were also identified. The IR band at 1073 cm^{-1} and the Raman band at 1067 cm^{-1} are assigned to the asymmetric stretching C–C–N mode. The corresponding C–C–N symmetric stretching mode is observed at 1001 cm^{-1} as a medium band. Its Raman counterpart is not identified. The DFT computation predicts this vibrational mode at 996 cm^{-1}. The very weak Raman band observed at 1342 cm^{-1} and the weak corresponding IR band located at 1320 cm^{-1}

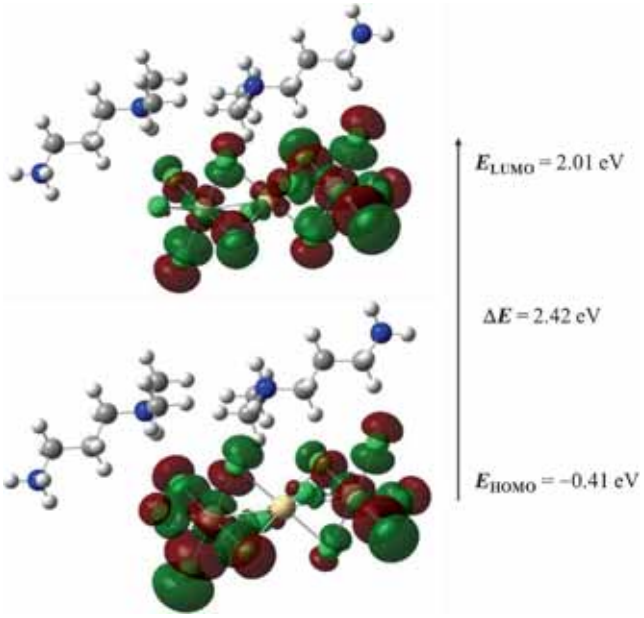

Figure 5. Frontier molecular orbitals (HOMO and LUMO) of $[(C_5H_{16}N_2)Cd_{1.5}Cl_5]$.

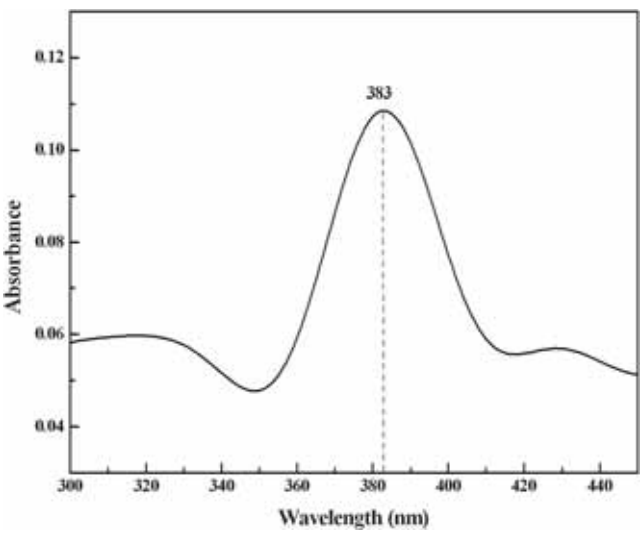

Figure 6. UV–visible spectrum of $[(C_5H_{16}N_2)Cd_{1.5}Cl_5]$.

Table 5. Observed and calculated vibrational frequencies (cm^{-1}) of $(C_5H_{16}N_2)Cd_{1.5}Cl_5$.

Observed			
FT-IR	FT-Ra	Calculated	Assignment with PED (%)[a]
3451wb	—	3361	ν(N–H)(94)
3185m	—	3107	ν_{as} (N–$H_{(3)}$)(79)
3121s	—	3098	ν_s(N–$H_{(3)}$)(83)
3069sh	—	3055	ν_{as}(C–$H_{(3)}$)(72)
3038s	—	3050	ν_{as}(C–$H_{(2)}$)(69)
3019s	—	3041	ν_{as}(C–$H_{(3)}$)(42)
2944m	—	2989	ν_s(C–$H_{(3)}$)(73) + ν_{as}(C–$H_{(2)}$)(22)
2899sh	—	2980	ν_s(C–$H_{(2)}$)(87)
2756w	—	2794	ν(N–H)(39)
2704vw			Overtone + combination
2552vw			Overtone + combination
2509vw			Overtone + combination
1896vw			Overtone + combination
1621w	1591w	1640	ν(C–N)(77)
1576vs	1580w	1565	ν(C–N)(18) + ν(C–C)(48)
1520s	1494m	1537	ρ (N–H)(38)
1478s	1481w	1456	δ (C–$H_{(3)}$)(48)
1460vs	1445s	1450	γ (C–$H_{(3)}$)(29)
1430m	1436w	1432	δ (C–$H_{(2)}$)(63)
—	1427vw	1423	δ (C–$H_{(2)}$)(13)
1411m	1396w	1414	Umbrella(81)
1373m	1372vw	1354	ω (C–$H_{(2)}$)(78)
1320w	1342vw	1307	ν(CNC)(47)
1283w	1306w	1259	γ (HCC)(24) + ν(C–N)(35)
1251w	1279w	1240	ν(C–N)(35)
1208w	1253m	1204	ν(C–C)(35)
—	1224w	1192	ξ(C–$H_{(2)}$)(11)
1177w	1124vw	1178	ρ(C–$H_{(2)}$)(78)
1094w	1109vw	1099	δ(CCC)(54) + ν(C–C)(23)
1073w	1067vw	1076	ν_{as} (CCN)(66)
1043w	1018vw	1044	ν(C–N)(65)
1001m	—	996	ν_s (CCN)(33)
974m	—	950	δ (CCC)(68) + γ (CCC)(14)
954m	914vw	937	γ(HCCC)(78)
911m	885vw	897	ν(C–C)(35)
850m	873vw	842	δ(C–C)(78)
798w	742s	787	δ_{as} (CCC)(28)
706s	575m	646	τ(CCCN)(41)
585vw	563w	594	ρ(C–$H_{(2)}$) (28) + δ(CNC)(34)
—	525w	560	τ(C–$H_{(2)}$)(20)
505w	510w	507	τ(C–$H_{(3)}$)(14) + γ (CCC)(10)
456sh	434w	463	τ(CCNC) (56)
432vw	384w	414	ν(CdCl): $\nu_3(F_{1u})$(73)
—	370vw	395	ν(CdCl): $\nu_3(F_{1u})$ (50)
—	361vw	391	ν(CdCl):$\nu_3(F_{1u})$(10) + δ(CNC)(86)
—	351w	355	ν(CdCl): $\nu_1(A_{1g})$(56)
—	306w	303	τ(C–$H_{(3)}$)(20) + γ(CCC)
—	272w	259	ν(CdCl): $\nu_2(E_g)$(31) + $\omega(CH_{(2)})$(24)
—	231vs	203	ν(CdCl): $\nu_2(E_g)$(28)
—	185m	169	δ(ClCdCl): $\nu_5(F_{2g})$(60)
—	159w	145	δ(ClCdCl): $\nu_5(F_{2g})$(43) + $\tau(CH_{(2)})$(14)
—	120m	115	δ(ClCdCl) : $\nu_5(F_{2g})$(72)
—	105s	104	ρ(ClClClCd)(42)

Abbreviations: s, strong; w, weak; v, very; sh, shoulder; b, broad; m, medium; ν, stretching; δ, in-plane bending; γ, out-of-plane bending; τ, torsion mode; ω, wagging; ρ, rocking; ξ, scissoring.
[a]Only contribution $\geq$ 10% listed.

can be assigned to the C–N–C stretching mode. The band observed at 585 cm^{-1} arises from the C–N–C symmetric bending mode coupled with the CH_2 rocking mode. This mode is well reproduced by DFT calculations at 594 cm^{-1}. The C–C–C vibrational bands were also identified. Table 5 presents a detailed assignment of all observed band related to the 3-dimethylammoniopropylammonium cation.

It is well known that hydrogen bonding brings a remarkable downward wavenumber shifts. The intermolecular hydrogen bonds give rise to broad bands, whereas bands arising from intramolecular hydrogen bonds are sharp and well resolved. By knowing the bond length, the strength of the hydrogen bond can be determined as strong (N···Cl below 3.21 Å) and weak (N···Cl above 3.21 Å) [26]. In the present structure, the $[Cd_{1.5}Cl_5]^{2-}$ anion and the 3-dimethylammoniopropyl-ammonium cation are connected through the N–H···Cl hydrogen bond. In fact, the decrease in the N–H stretching mode (2756 cm^{-1} (IR)) confirms the presence of these hydrogen bonds. In addition, each hydrogen atom of the ammonium group participates in the formation of N–H···Cl hydrogen bonds with one chlorine atom of $CdCl_6$ octahedra. The bond lengths of these hydrogen bonds vary in the range 2.351–2.702 Å. They are responsible for the broad IR band centred around 3161 cm^{-1} and the reduction in the N–H stretching wavenumbers.

4.6 *Thermal behaviour*

From the TG–DTA thermograms (figure 9), we deduce that the anhydrous compound decomposes in the range 303–450°C, with the maximum elimination of NH_3 at 371°C.

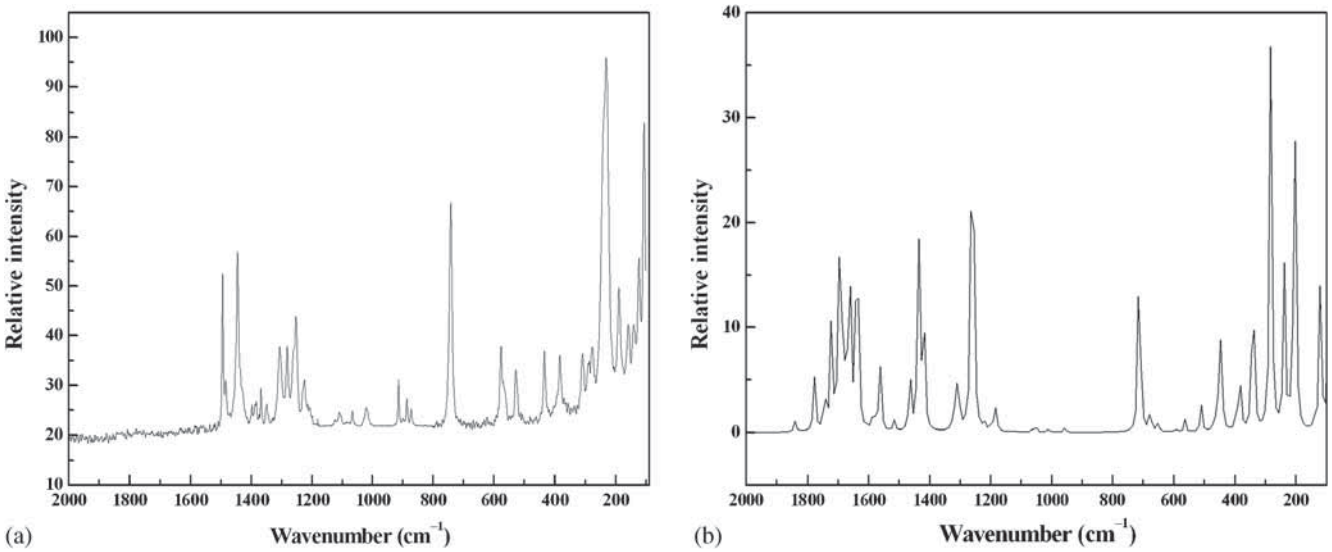

Figure 7. FT-Raman spectra of $[(C_5H_{16}N_2)Cd_{1.5}Cl_5]$: (**a**) observed and (**b**) calculated.

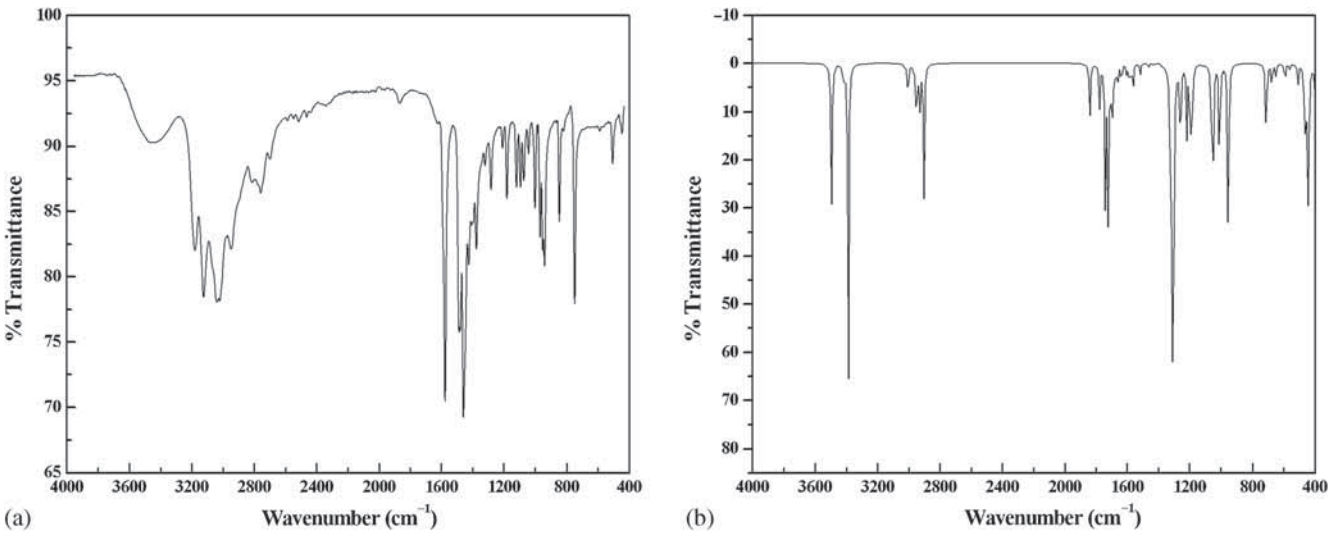

Figure 8. IR spectra of $[(C_5H_{16}N_2)Cd_{1.5}Cl_5]$: (**a**) observed and (**b**) calculated.

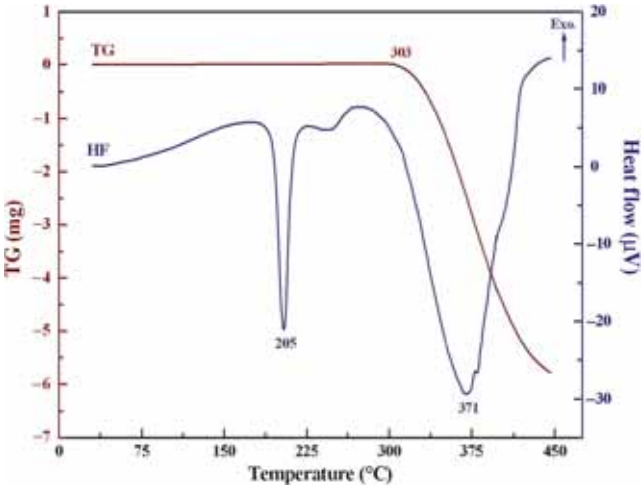

Figure 9. TG–DTA thermograms of $[(C_5H_{16}N_2)Cd_{1.5}Cl_5]$.

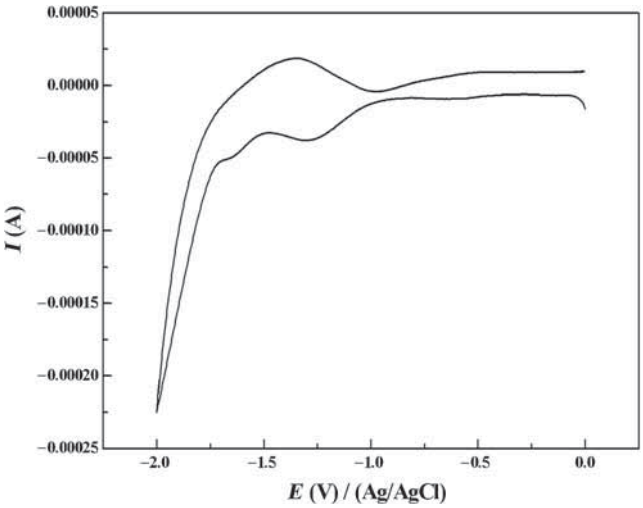

Figure 10. Cyclic voltammogram of $[(C_5H_{16}N_2)Cd_{1.5}Cl_5]$.

Within this temperature range, a rather bad smell emanates from the resulting black compound. The DTA curve shows a strong endothermic peak occurring in the temperature range 185–220°C. This peak may be ascribed to the melting. The melting of the compound is confirmed by an additional thermal treatment in a separate carbolite furnace with heating at 5°C min^{-1} from room temperature to 205°C. The resulting compound is a white liquid.

4.7 *Electrochemical measurements*

In order to discuss the redox properties of our compound, the cyclic voltammogrammetry was performed in a 10^{-3} M sample solution in acetonitrile (CH_3CN), containing tetrabutylammonium tetrafluoroborate (TBAF) as supporting electrolyte. The range of potential studied was between 0 and −2.25 V with a scan rate of 100 mV s^{-1}. Two successive reduction waves at the negative potential region were observed, demonstrating that electroactive species can have two different oxidation states (figure 10). Therefore, the observed waves can be respectively assigned to Cd(II)/Cd(I) ($Ep_c = -1.30$ V, $Ip_c = -3.76 \times 10^{-5}$ A) and Cd(I)/Cd(0) ($Ep_c = -1.64$ V, $Ip_c = -4.83 \times 10^{-5}$ A) couple processes [40,41]. In addition to these waves, there is an oxidation wave at −1.35 V, which appeared when measuring in the opposite direction. Thus, it does not correspond to the Cd(0)/Cd(II) process. The peak separation between anodic and cathodic peak potentials (ΔE) was the highest for the scan rates of 100 mV s^{-1}. The large potential difference separation (ΔE) at the glassy-carbon electrode is indicative of an electrochemically irreversible process.

5. Conclusions

In the present work, a new mono-dimensional hybrid organic–inorganic transparent crystal $(C_5H_{16}N_2)Cd_{1.5}Cl_5$ was synthesized. X-ray characterization, UV–vis study and thermal analysis of the compound were reported. Detailed vibrational spectral analysis was performed by combining experimental and theoretical information using DFT. Hirshfeld surface analysis and 2D fingerprint plots were generated, making the understanding of the N–H···Cl intermolecular interactions easily. The HOMO–LUMO energy gap explains the eventual charge transfer interactions taking place within the molecule.

Acknowledgements

Grateful thanks are expressed to Dr Amor Jouini (Laboratoire de Chimie du Solide, Faculté des Sciences de Monastir, Tunisia) for the assistance in single-crystal X-ray diffraction data collection.

Electronic Supplementary Material

Supplementary Material pertaining to this article is available on the *Bulletin of Materials Science* website (www.ias.ac.in/matersci).

References

[1] Calabrese J, Jones N L, Harlow R L, Herron N, Thorn D L and Wang Y J 1991 *J. Am. Chem. Soc.* **113** 2328

[2] Mitzi D B, Chondroudis K and Kagan C R 2001 *IBM J. Res. Dev.* **45** 29

[3] Gebauer T and Schmid G 1999 *Z. Anorg. Allg. Chem.* **625** 1124

[4] Bourdeau C L, Chanh N B, Duplessix R and Gallois B 1993 *J. Phys. Chem. Solids* **54** 349

[5] Puget R, Jannin M, de Brauer C and Perret R 1991 *Acta Crystallogr. C* **47** 1803

[6] Amamou W, Feki H, Chniba-Boudjada N and Zouari F 2014 *J. Mol. Struct.* **1059** 169

[7] Hajji M, Gharbi A and Guerfel T 2014 *J. Inorg. Organomet. Polym. Mater.* **24** 766

[8] Xu R 2009 *Acta Crystallogr. E* **65** m951

[9] Glaoui M, Zeller M, Jeanneau E and Ben Nasr C 2010 *Acta Crystallogr. E* **66** m895

[10] Amamou W, Guerfel T and Mhiri T T 2013 *J. Inorg. Organomet. Polym. Mater.* **23** 1511

[11] Hlel F, Rheim A, Guerfel T and Guidara K 2006 *Z. Naturforsch. B* **61** 1002

[12] Spackman M A and Jayatilaka D 2009 *CrystEngComm* **11** 19

[13] McKinnon J J, Jayatilaka D and Spackman M A 2007 *Chem. Commun.* 3814

[14] Harms K and Wocadlo S 1995 *XCAD4* (Germany: University of Marburg)

[15] Sheldrick G M 2008 *Acta Crystallogr. A* **64** 112

[16] James W H, Buchanan E G, Müller C W, Dean J C, Kosenkov D, Slipchenko L V, Guo L, Reidenbach A G, Gellman S H and Zwier T S 2011 *J. Phys. Chem. A* **115** 13783

[17] Young D C 2001 *Computational chemistry*: *a practical guide for applying techniques to real-world problems* (New York: John Wiley and Sons) p 187

[18] Sert Y, Al-Turkistani A A, Al-Deeb O A, El-Emam A A, Ucun F and Çırak Ç 2014 *Spectrochim. Acta A* **120** 97

[19] Dennington R, Keith T and Millam J 2009 *GaussView Version 5* Semichem Inc Shawnee Mission KS

[20] Frisch M J, Trucks G W, Schlegel H B *et al* 2009 *Gaussian 09 Revision A1* (Wallingford CT: Gaussian Inc.)

[21] Jamróz M H 2013 *Spectrochim. Acta A* **114** 220

[22] Merrick J P, Moran D and Radom L 2007 *J. Phys. Chem. A* **111** 11683

[23] Wolff S K, Grimwood D J, McKinnon J J, Turner M J, Jayatilaka D and Spackman M A 2012 *Crystal Explorer 30* (Perth, Australia: University of Western Australia)

[24] Allen F H, Kennard O, Watson D G, Brammer L, Orpen A G and Taylor R 1987 *J. Chem. Soc. Perk. T.* **2** 1

[25] Baur W H 1974 *Acta Crystallogr. B* **13** 1195

[26] Pimental G C and Mc Clellan A L 1960 *The hydrogen bond* (San Fransisco and London: W H Freeman and Company)

[27] Spackman M A and Byrom P G 1997 *Chem. Phys. Lett.* **267** 215

[28] Fukui K 1982 *Science* **218** 747

[29] Padmaja L, Ravikumar C, Sajan D, Joe I H, Jayakumar V S, Pettit G R and Nielsen O F 2009 *J. Raman Spectrosc.* **40** 419

[30] Ravikumar C, Joe I H and Jayakumar V S 2008 *Chem. Phys. Lett.* **460** 552

[31] Fleming I 1976 *Frontier orbitals and organic chemical reactions* (New York: John Wiley and Sons)

[32] Lee S K and Choi H S 2001 *Bull. Kor. Chem. Soc.* **22** 463

[33] Nakamoto K 2009 *Infrared and Raman spectra of inorganic and coordination compounds part a*: *theory and applications in inorganic chemistry* 6th edn (Wiley: Hoboken)

[34] Litivinow G 1992 *Proceedings of the XII International Conference on Raman Spectroscopy* (Germany: Wurzburg)

[35] Furie K, Mohacek V, Bonifacic M and Stefanic I 1992 *J. Mol. Struct.* **267** 39

[36] Lau G and Wang H 1990 *Spectrochim. Acta A* **46** 1204

[37] Snyder R G and Scharchtschneider J H 1964 *Spectrochim. Acta A* **20** 853

[38] Sundaraganesanet N, Anand B, Meganathan C, Dominic Joshua B and Saleem H 2008 *Spectrochim. Acta A* **69** 198

[39] Krishnakumar V, Surumbarkuzhali N and Muthunatesan S 2009 *Spectrochim. Acta A* **71** 1810

[40] Deveci P, Taner B, Kllç Z, Solak A O, Arslan U and Özcan E 2011 *Polyhedron* **30** 1726

[41] Torres E L and Mendiola M A 2005 *Inorg. Chem.* **49** 7638